Supporting Information

Chemical Kinetics of Nanoparticles in Emulsion State during Phase-Transfer Synthesis

Yu Jin Kim[1], Junghoon Kim[2], Jungho Kim[2], Hyunjung Kim[1]*

[1]Department of Physics, Sogang University, Seoul, Korea

[2]Laboratory of Molecular and Cellular Biology, Department of Life Science, Sogang University, Seoul, Korea

ADDITIONAL EXPERIMENTS

Additional Material

Nile red (BioReagent, ≥ 98.0 %) as a fluorescence material was purchased from Sigma-Aldrich and used without further purification.

General Characterization

The number or volume distribution of particle size for synthesized colloids was measured by dynamic light scattering (DLS) on a Zetasizer Nano-ZS (Malvern Instr. Co). The particle solutions were filled into a quartz square cuvette (DTS0012, 1.08 mL), and they were scanned with 17 runs each at room temperature. The equilibrium time and a measurement angle were 120 s and 173° backscatter, respectively.

The particle structure, including size, was confirmed by transmission electron microscopy (TEM) operating at an acceleration voltage of 200 kV (JEOL-2100F or JEM-F200 equipped with a high-angle annular dark-field (HAADF)). The high-resolution (HR) TEM images were obtained via focus and magnification variations. The particle dispersions are diluted 1/7 in distilled water, and they were drop-casted onto the ultrathin lacy carbon or carbon support film grids (400 mesh, Copper). Samples were dried in the air for over 48 h before loading into the TEM instrument.

UV-vis absorption spectra with a baseline correction were scanned using a Cary 50 UV-Vis-NIR spectrometer. Scan speed and mode were 100 nm/min and medium, respectively. The data interval was 0.02 nm. Colloidal solutions were filled in a quartz cuvette with a path length of 10 mm and measured.

Confocal microscope images for emulsion morphologies with two phases of oil-water were obtained using a Leica TCS-SP8 UV/visible laser confocal microscope with a Plan-Apochromat

×63. The CTAB solutions dissolved in chloroform were stained with Nile red molecules (0.1 mg mL^{-1}) for visualization of the oil droplets. The emulsion solutions (2 μl) were dropped onto the slide-glass and covered with a thin cover-glass. The samples were mounted onto the sample stage and contacted with the Plan-Apochromat. A 532 nm laser was applied to excite the Nile red and visualized microscopic structures (Z-zoom to 2.50) were captured from the emitted light. The measured images were generated using ImageJ software.[S1]

Small-angle X-ray scattering (SAXS) measurements were conducted at the 4C SAXS-Ⅱ beamline of the PLS-Ⅱ synchrotron facility, Pohang Accelerator Laboratory (Pohang, Korea). The X-ray beam with an energy of 16.09 keV was used, and scattering data were collected with a two-dimensional charged-coupled detector (CCD: model Rayonix 2D SX 165). The beam continuously exposed every 5 s with a beam-off time of 5 s interval and sample-to-detector distance (SDD) was set to 4.0 m (confidence interval: 0.065 $Å^{-1} < q < 0.1$ $Å^{-1}$). The scattering angles were calibrated by using a pre-calibrated Ti-SBA-15 (Sigma-Aldrich) and silver behenate (Tokyo Chemical Industry) as standards. Experiments were performed *in situ* during the emulsion/solvent evaporation synthesis. Synthesis equipment (homogenizer – Ultrasonic Processor VCX-750W) and a flow cell (HAMILTON – Microlab 600) were connected to transparent flow lines, and the solution continuously flowed with a 7 μL/s rate. A capillary cell (a thickness of 0.01 mm and an external diameter of 1.0 mm, Charle Supper Company) was placed in a metal holder mounted in the X-ray beam path, and thus all SAXS data were recorded at the same position and had a cell effect. For the static data (structures of CTAB molecules, FigureS15), a solution was filled into the capillary cell and measured with an exposure time of 10 s. When the change of the solution, the cell was washed to di-water and acetone 3 times. For the background

subtraction, SAXS patterns for the buffer solutions (CF, water, or CF/water mixed solution) were separately measured and subtracted from particle solutions in SAXS data treatment.

Synthesis of CTAB-decorated AuNPs treated with non-chloride solvents (Figure S6)

Cetyltrimethylammonium bromide (CTAB)-decorated gold nanoparticles (AuNPs) were synthesized in the same manner as that described in the Experimental Section of the main text except for using chloroform (CF). The CF oil phase was replaced with toluene, tetrahydrofuran (THF), or cyclohexane. The particles were synthesized with two CTAB concentrations (1.37 mM and 0.17 mM).

Synthesis of CTAB-covered AuNPs in the aqueous phase (Figure S8)

CTAB with various concentrations and gold AuNPs (1 mL) were dissolved in deionized water (di water, 3 mL) together and blended by magnetic stirring (750 rpm) over 1h.

Preparation of aqueous CTAB solutions (Figure S9)

CTAB was dissolved in di water (4 mL) with various concentrations by magnetic stirring (750 rpm) for 60 min.

Structure determination of CTAB molecules synthesized via the emulsion/solvent evaporation method (Figure S10)

CTAB molecules were dissolved in CF (1 mL) with various concentrations. An opaque mixture was formed by emulsifying the CF solution in a water phase (4 mL) with a homogenizer (Ultrasonic Processor VCX-750W, 1/4" tip, 23 % amplitude). After 85 min, a transparent aqueous CTAB dispersion was obtained.

Effect of the CF phase on the gold nanoparticles in the emulsion/solvent evaporation synthesis (Figure S11-S12)

A CF solution of 1 mg mL^{-1} was prepared. Aqueous AuNP solution (1 mg mL^{-1}) was diluted in di water of 3 mL. The AuNP solution was vigorously shaken for 3 min by the same homogenizer mentioned above. After the time, the CF oil phase was slowly dropped into the aqueous AuNP dispersion under the emulsification process, and then the mixture was blended for 150 min. The homogeneous CF-treated AuNP solution was finally obtained, which was transparent and colorless. After the synthesis, to remove excess oil solvent, the dialysis procedure was conducted using a dialysis tube (10 kDa membrane tube) in 3.8 L of di-water for 30 h.

The theoretical calculations for the number of CTAB molecules covered AuNPs in two models.

The CTAB concentrations were categorized into low, medium, and high with 0.17 mM, 0.51mM, and 1.37 mM, respectively. Through the theoretical calculations, the total number of CTAB molecules that are covered on the AuNPs can be estimated. In two CTAB models[S2-S3], the theoretically required CTAB molecules are calculated, and they are evaluated with the experimentally used CTAB molecules in three different concentrations.

From the CTAB and AuNP structures, the theoretical calculations are determined.

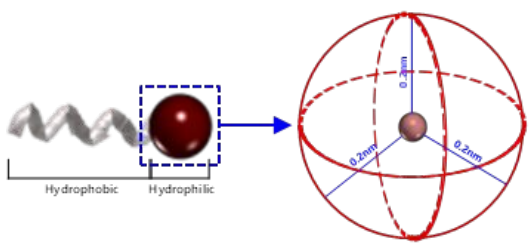

[1]

A CTAB structure has a head sphere for the hydrophilic part and a hydrophobic tail. The radius of the head is 0.2 nm.

We used an aqueous AuNP solution with ~ 6.54×10^{11} particles/ml concentration and ca. 20 nm in diameter,

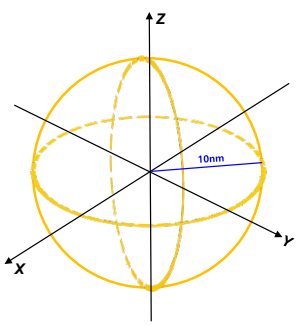

4π

The number of AuNPs in 1 mL = 6.54×10^{11}

Radius (r) of an AuNP = 10 nm.

The surface area of an AuNP is calculated to a circle model,

$r^2 = 400 \times \pi\ nm^2$

Based on the two structures, the total number of CTAB molecules that are covered on the AuNPs is calculated. The CTAB molecules can be covered in two models, i.e., bilayer or micelle structure.

(1) Bilayer structure

When the head of the CTAB molecule is attached to the AuNP surface, the maximum contact area can be considered to be a hemisphere contact.

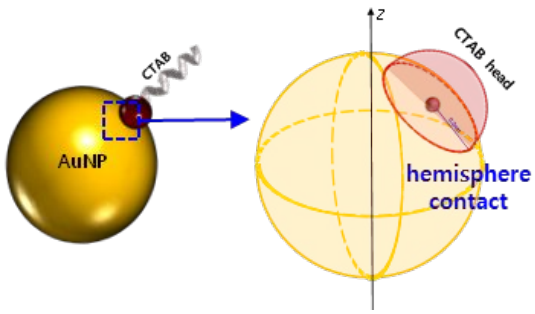

The contact area of a CTAB head on the AuNP surface = $\pi r^2 = \pi \times (0.2\ nm)^2 = 0.04 \times \pi\ nm^2$

The total number of CTAB molecules covered on an AuNP surface is calculated to the surface area of an AuNP divided by the contact area of a CTAB molecule,

$= 400 \times \pi\ nm^2\ /\ 0.04 \times \pi\ nm^2 = \sim\ 1.0 \times 10^4$

For the bilayer structure, the amount that CTAB molecules are needed is double. Thus,

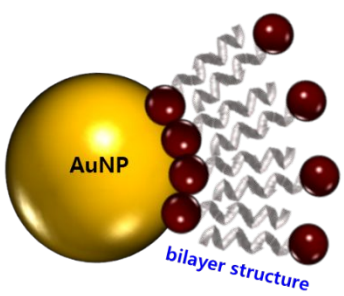

The number of CTAB molecules for an AuNP

$= \sim\ 2.0 \times 10^4$

Finally, the total number of CTAB molecules that are covered on all AuNPs

$= 6.54 \times 10^{11}\ (total\ AuNP\ particles) \times 2.0 \times 10^4$

$= \sim\ \mathbf{1.30 \times 10^{16}}$

(2) Micelle structure

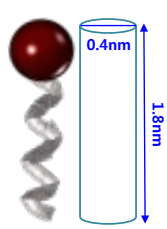

The volume of a CTAB = $\pi r^2 \times h = 0.072 \times \pi\ nm^3$

For the micelle model, it corresponds to a high CTAB amount over critical micelle concentration.

CTAB molecules can form a micelle structure, which is attached to the AuNP.

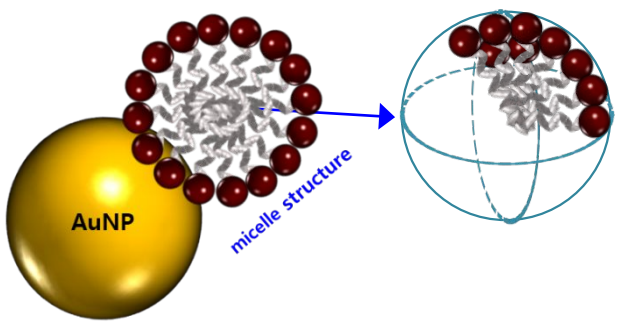

The volume of a CTAB micelle structure is calculated with the 1.8 nm length of the CTAB molecule as a micelle radius. It is the minimum volume that CTAB molecules can form a micelle.

$$= \frac{4}{3}\pi r^3 = \frac{4}{3} \times \pi \times (1.8\,nm)^3 = 7.776 \times \pi\,nm^3$$

The total number of CTAB molecules in a micelle is calculated to the volume of a CTAB micelle divided by the volume of a CTAB molecule, $7.776 \times \pi\,nm^3 \;/\; 0.072 \times \pi\,nm^3 = \sim 108$.

The maximum contact area of the CTAB micelle structure is when the micelle has a hemisphere contact.[S4]

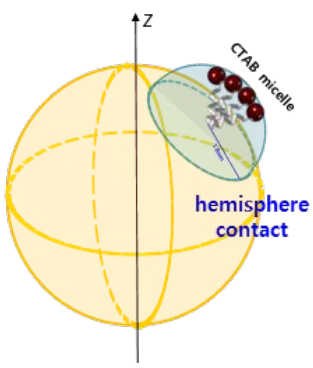

The contact area of a CTAB micelle on the AuNP surface

$$= \pi r^2 = \pi \times (1.8\,nm)^2 = 3.24 \times \pi\,nm^2$$

The total number of CTAB micelles covered on an AuNP surface is calculated to the surface area of an AuNP divided by the contact area of a CTAB micelle, $400 \times \pi\,nm^2 \;/\; 3.24 \times \pi\,nm^2 = \sim 123$

The number of CTAB molecules for an AuNP is $108 \times 123 = \sim 1.328 \times 10^4$.

Finally, the total number of CTAB molecules that are covered on all AuNPs,

$$= 6.54 \times 10^{11}\,(total\ AuNP\ particles) \times 1.328 \times 10^4$$

$$= \sim \mathbf{8.69 \times 10^{15}}$$

Therefore, we understand that the required CTAB molecules to cover all AuNPs, in theory, are ~ 1.30×10^{16} for the bilayer structure and ~ 8.69×10^{15} for the micelle structure. Experimentally used CTAB molecules can be calculated to 1.0238×10^{20} for 0.17 mM, 3.0712×10^{20} for 0.51 mM, and 8.2503×10^{20} for 1.37 mM of CTAB concentration based on the Avogadro's number. It means that the categorized CTAB concentrations that occur a cracking phenomenon of AuNP or are effectively phase-transferred to the AuNP to create a CTAB-covered AuNP structure are all excess conditions than the theoretical amount in fully CTAB-covered AuNPs.

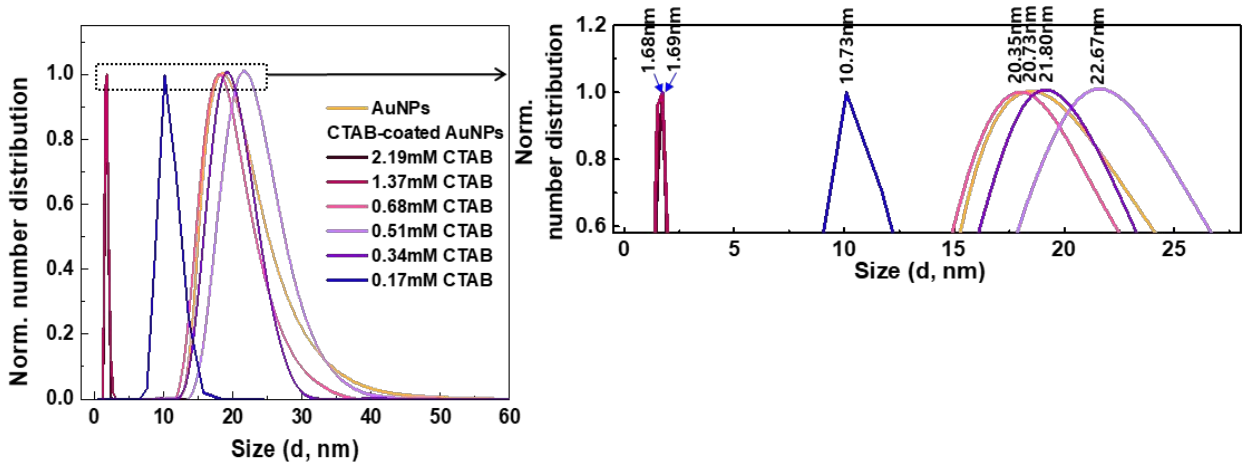

Figure S1. Detailed distribution positions with structure size from Figure 1b.

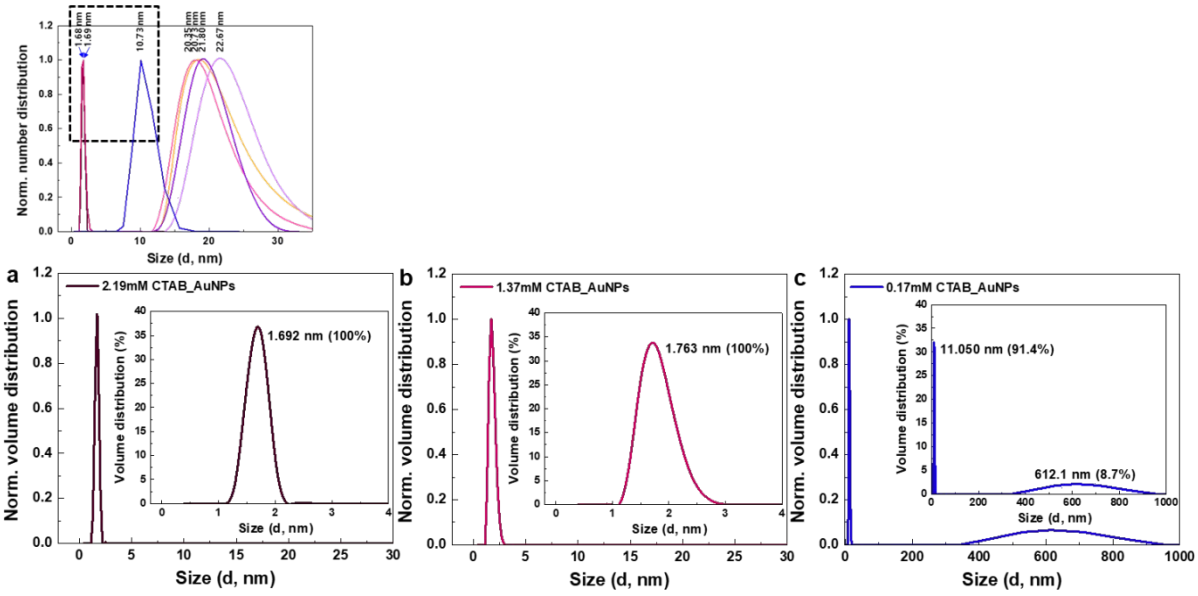

Figure S2. Plots for volume distribution vs. size of AuNPs determined by DLS. Inset figures and numbers are non-normalized DLS results and Z-average diameters calculated from the DLSs, respectively.

To understand the dynamic light scattering (DLS) data obtained from Figure 1b, we investigated volume distributed DLS results for the samples showing the cracking phenomenon of AuNPs. As shown in Figure S2 a and b, we find that ca. 1.7 nm-sized particles were observed with a volume distribution of 100 %. In the 0.17 mM of CTAB condition (c), volume distribution over 91 % was revealed with around 11 nm-sized structure. They indicate that almost all nanoparticles are from the decomposition of AuNPs.

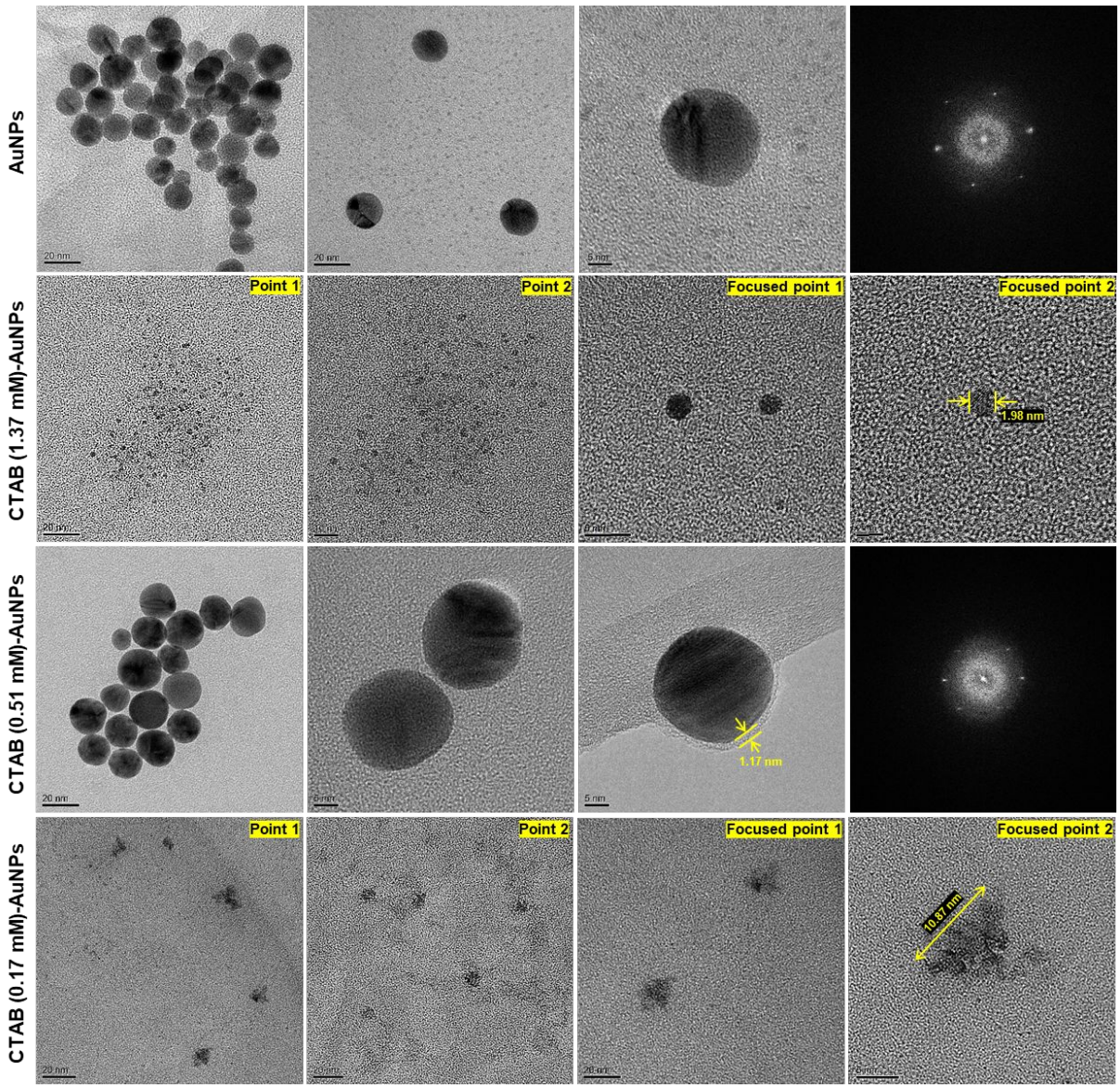

Figure S3. Big-sized TEM images for targeting samples with 1.37 mM, 0.51 mM, and 0.17 mM of CTAB concentration including pure AuNPs: first row – original AuNPs, second row – 1.37 mM, third row – 0.51 mM, and fourth row – 0.17 mM. Point 1 and Point 2 mean two different measurement points. Two images with a black background exhibit FFT diffraction patterns for the gold nanoparticle.

The above TEM images show considerably different AuNP structures. In the first line, we can find that we have certainly used ca. 20 nm-sized AuNPs. The split AuNPs with ~ 2 nm-sized spherical structure was shown in the 1.37 mM of CTAB condition, whereas assembled structures of ca. 11 nm containing tiny particles were observed in the 0.17 mM of CTAB concentration. The 0.51 mM of CTAB concentration allowed a CTAB-covered particle

structure, and its layer showed ca. 1.2 nm.

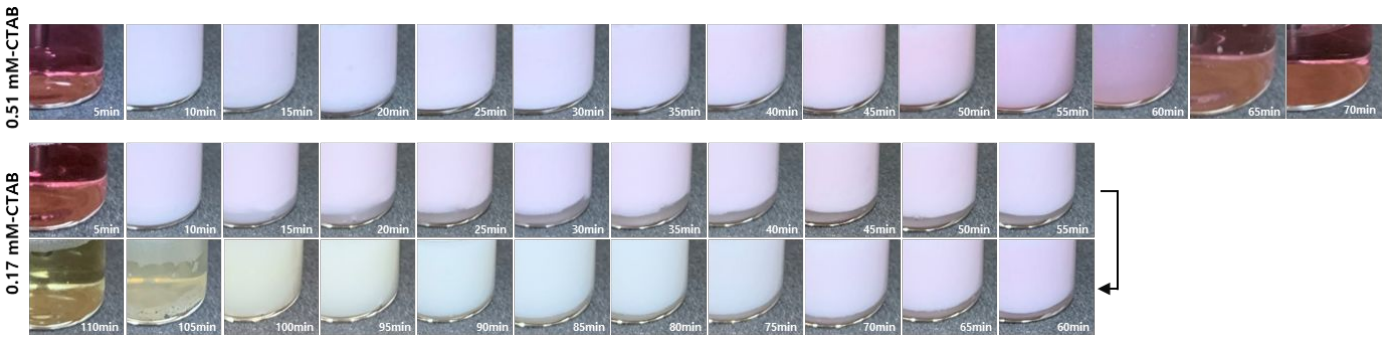

Figure S4. Full-color variations of CTAB-loaded AuNP solutions with a time interval of 5 min: upper row section – 0.51 mM and lower row section – 0.17 mM of CTAB concentration.

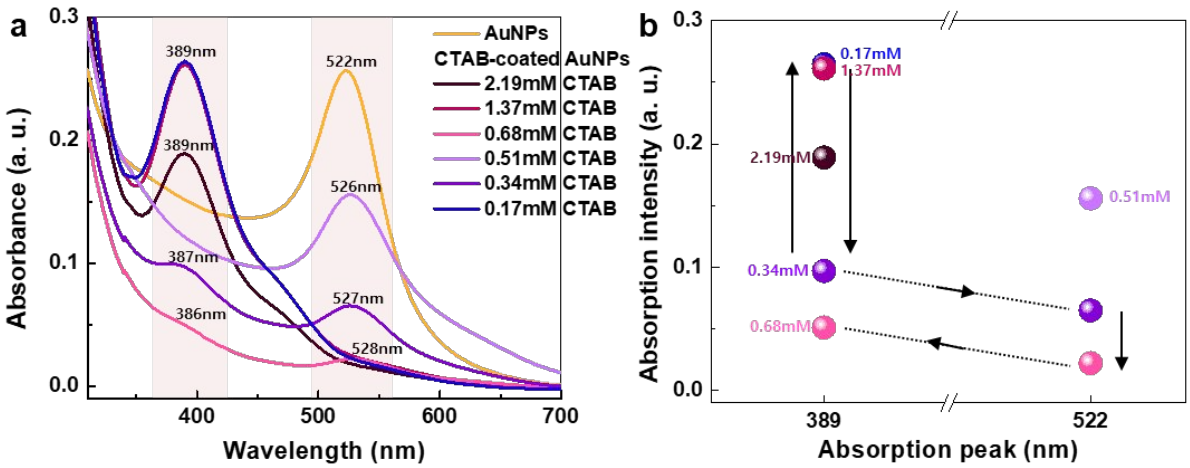

Figure S5. (a) UV-vis absorption spectra with peak positions for CTAB-decorated AuNPs as a function of CTAB concentration and (b) a visualized trend at ca. 389 nm and 522 nm.

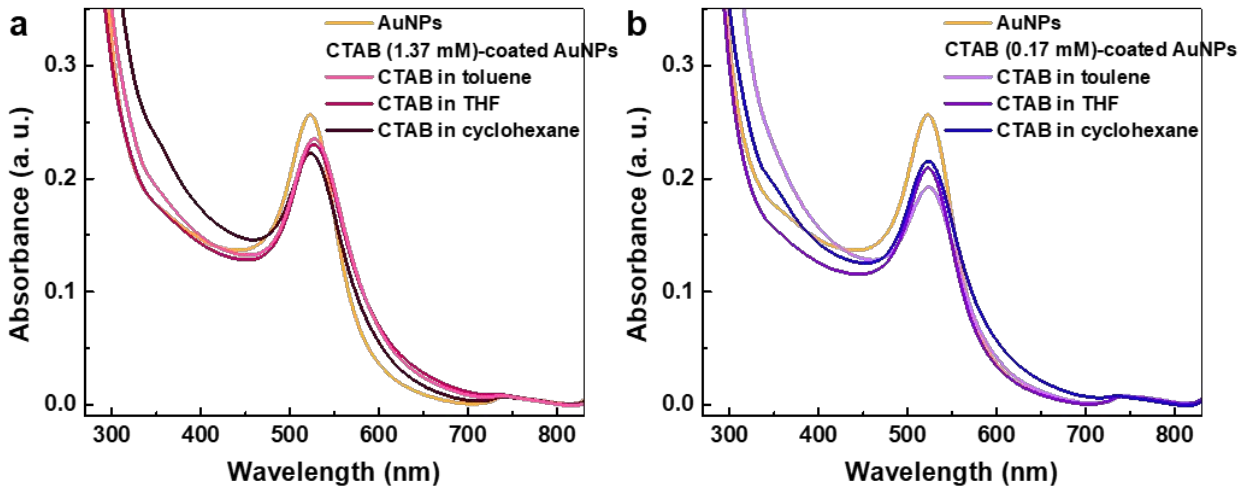

Figure S6. UV-vis absorption spectra with LSPR bands for synthesized CTAB-covered AuNPs using non-chloride solvents (toluene, THF, and cyclohexane) in the oil phase: 1.37 mM (a) and 0.17 mM (b) of CTAB condition (THF: tetrahydrofuran).

When we investigated the role of the CF in the emulsion synthesis at the 0.17 mM of CTAB concentration, the UV-vis absorption spectra also showed a CTAB-covered AuNP structure in all processing solvents in the oil phase (Figure S6b). In the low CTAB concentration showing the cracking phenomenon of the AuNPs, the CF solvent also has the main role in determining the colloidal structure in the aqueous phase.

Additionally, we carefully conducted other experiments to verify the CF issue in the emulsion/solvent evaporation synthesis. The effects on the structural variation of AuNPs by other external parameters or synthesis conditions were investigated. We first observed variations of AuNP solutions processed with different agitation methods and heating conditions (the processing temperatures were determined to the same conditions of synthesis of CTAB-loaded AuNP). When the solutions processed with a magnetic stirring under three different temperatures, 80 °C, 90 °C, and 95 °C, they showed the same AuNP structure in the UV-vis absorption spectra and size distribution results determined by DLSs (Figure S7a and S7b). In the homogenizer-processed samples, ca. 20 nm-sized AuNPs were not also changed in the structure and size, as shown in Figure S7c and S7d. From all results, they indicate that the agitation methods and temperatures over 80 °C are not factors to affect the cracking of AuNPs.

As a second proof, we synthesized CTAB-loaded AuNPs in the water to investigate the decomposition of AuNPs by the interactions with CTAB molecules. The synthesized particles showed localized surface plasmon resonance (LSPR) bands corresponding to AuNPs[S5] and a CTAB molecule-covered structure, which can be confirmed in Figures S8b and S8c. In this experiment, we can also understand that the interactions between CTAB and AuNPs do not generate the gold split.

The following experiments demonstrate that the Soret peak at ca. 389 nm in the UV-vis absorption spectra and the sizes from DLSs in Figure 2b and Figure 1b are not arising from self-assembled CTAB molecules. When CTAB molecules with various concentrations were dispersed in water (Figure S9a), the specific structures were not shown in the UV-vis absorption spectra, particularly in the Soret band region (Figure S9b). DLS results measured with two different material models exhibited over 29 nm-sized structures in the PMMA (Figure S9c). In the PS latex material model, the range of calculated diameter values has not covered

the size of cracking AuNPs (Figure S9d). We then investigated the structure of CTAB molecules processed by the emulsion/solvent evaporation method (Figure S10a). When the molecules were dispersed in chloroform (CF), and were synthesized into the water phase, they did not also show a specific assembled structure, as shown in Figure S10c. For the size distributions (Figure S10d and S10e), particularly in the 1.37 mM and 0.71 mM of CTAB concentrations, they have similar values with the size of the cracked AuNPs. However, we can find that the exact values are manifestly different. Despite their small numbers in size, we can understand that the ca. 1.7 nm- and ca. 11 nm-sized structures are from the split AuNPs because the synthesized CTAB structures did not show the Soret peak at the violet in the wavelength in the absorption spectra.

From the proof data, it verified that the results in Figure 1b and Figure 2b, and corresponding the suggested scenario for the decomposition of AuNPs are mainly caused by the CF phase. To directly understand the CF phase in the synthesis, we finally conducted the emulsion/solvent evaporation process with the aqueous AuNP phase and the CF oil phase. A transparent blend solution with pink color at the early synthesis stage was rapidly changed to an opaque solution, which was kept until 105 min. After that time, the solution was gradually changed with transparency, and the transparent solution with colorless was obtained (Figure S11). In the color variation of the solution, we can understand that the process has emulsion states by the interactions between the water and CF phase, and the final solution has one phase of the water. It means that we can argue the exact effect of the CF phase on the AuNPs in the synthesis. Indeed, the structure of 20 nm-sized AuNPs was entirely collapsed (Figure S12c and S12d); the absorbances showed smooth bands without specific peaks in both UV-vis absorption spectra of the synthesized solution and its dilute condition. They exhibited quite a broad shoulder band in the range of 530 – 600 nm. Besides, when we added CTAB molecules with

1.37 or 0.17 mM concentration, we can find that the cracked AuNPs in the water phase do not have chemical interactions with CTAB molecules after the evaporation of the CF phase. It means that the creation of Au(III)Br_4-CTA complex occurred in the synthesis from the interactions between AuNPs and CF phase including CTAB molecules, and thus the role of the CF phase and the formation of the new complex were verified.

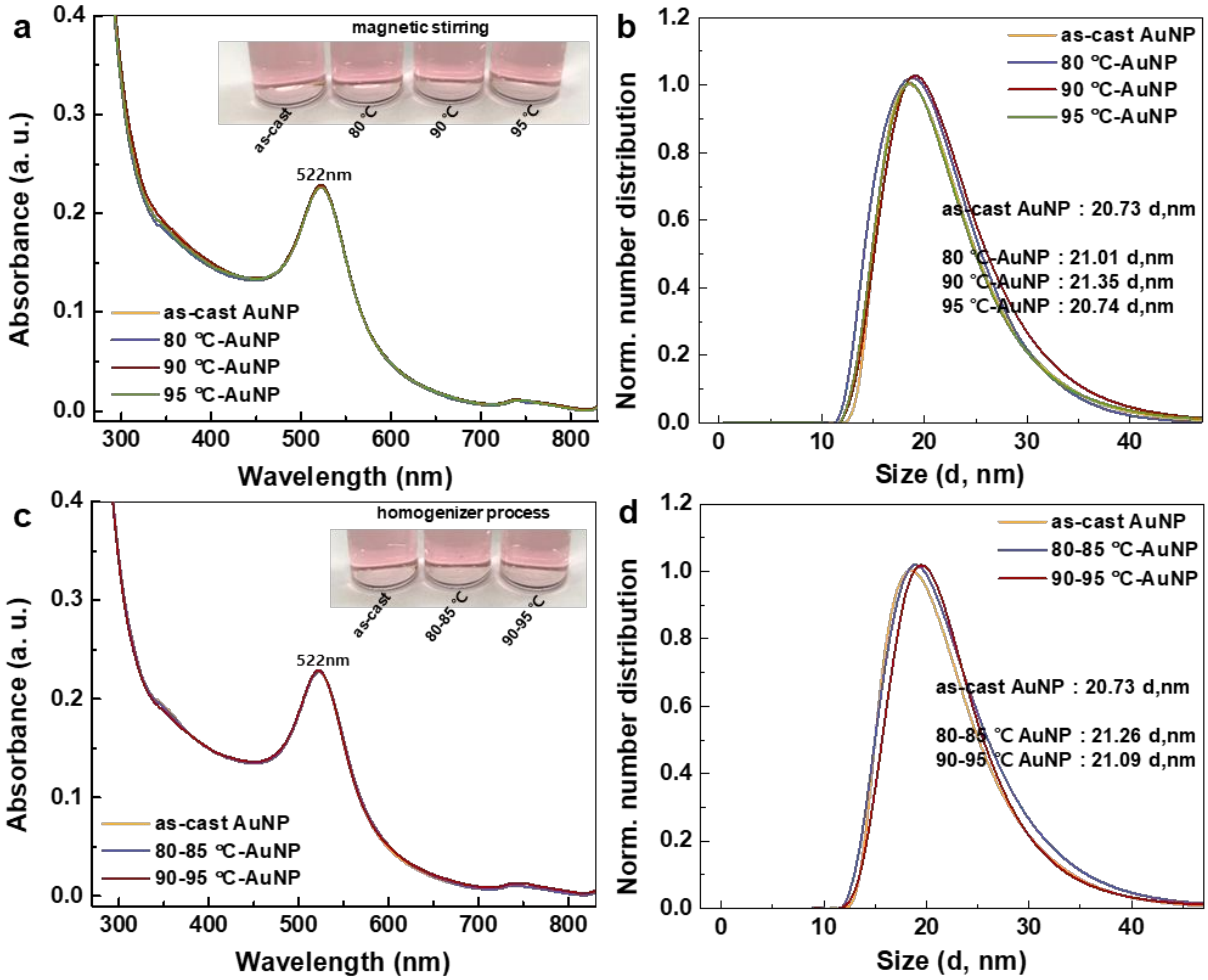

Figure S7. Aqueous AuNP solutions with two different agitation – magnetic stirring (a and b) and using a homogenizer (c and d) and processed with various temperatures: UV-vis absorption spectra showing LSPR bands (a and c, insets: visualization of AuNP solution with the different process) and DLS results for normalized number distribution vs. size.

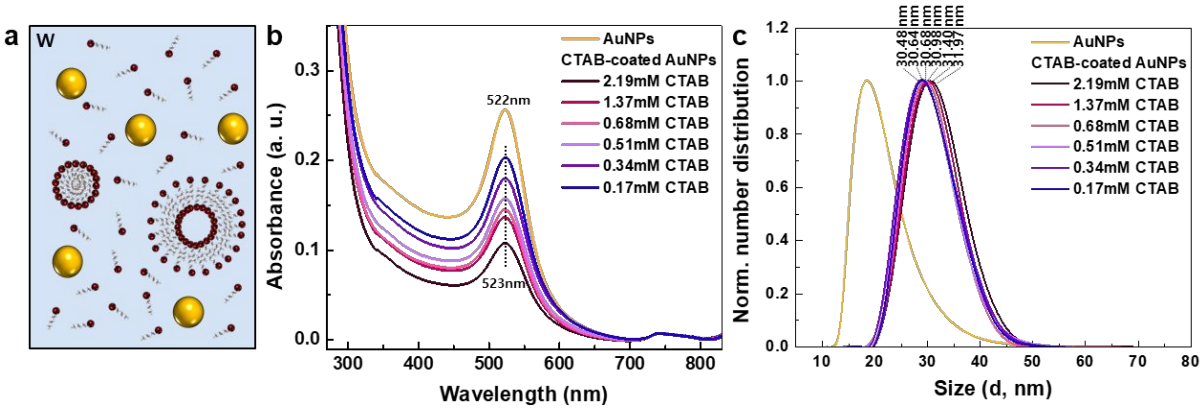

Figure S8. CTAB-covered AuNPs as a function of CTAB concentration synthesized in aqueous phase: (a) illustration of synthesis, (b) UV-vis absorption spectra, and (c) size distributions measured by DLS.

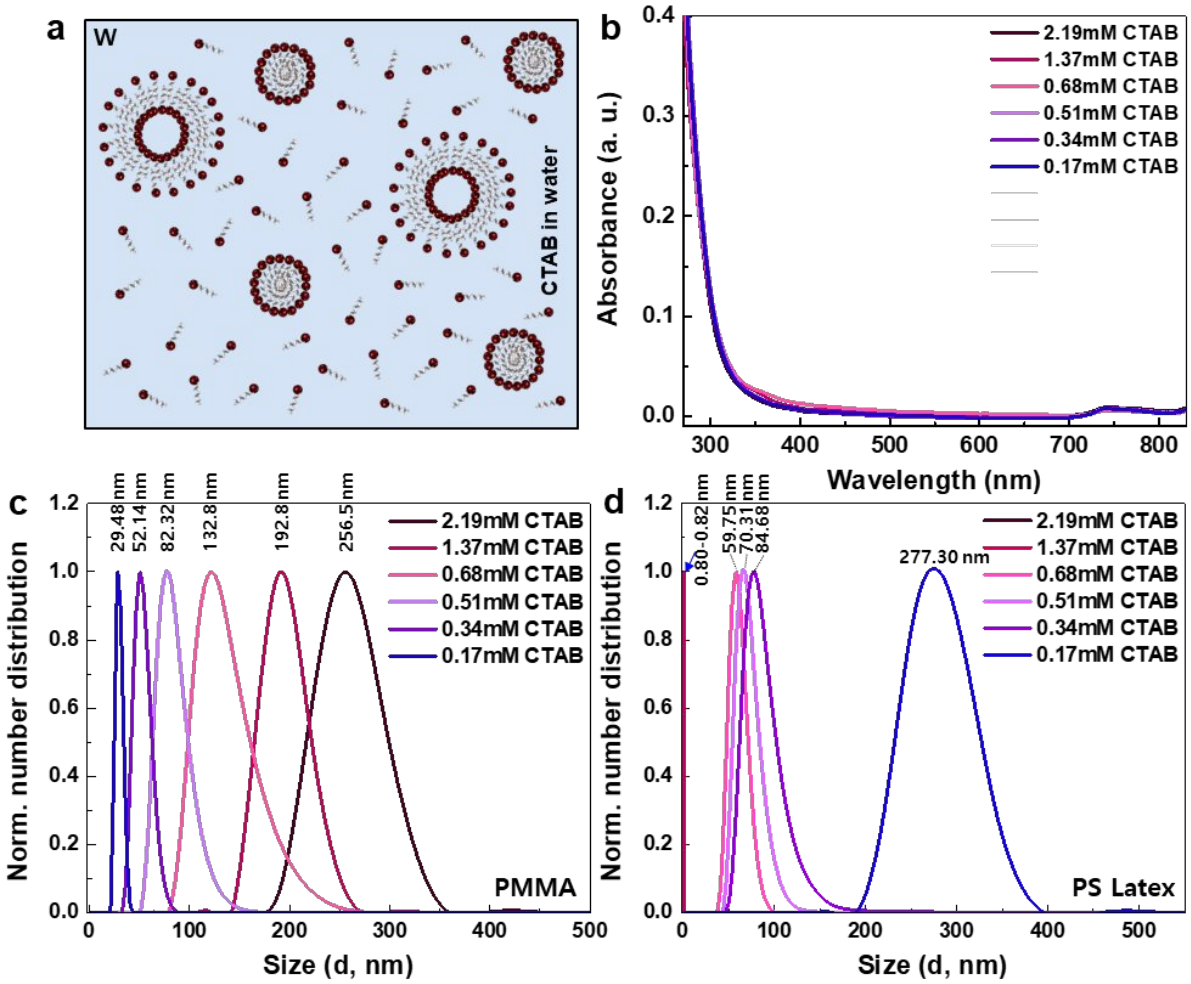

Figure S9. Aqueous CTAB dispersions with different surfactant amounts: (a) synthesis picture, (b) UV-vis absorption spectra, (c and d) DLSs for number distribution measured with two different structure models – PMMA (c) and PS latex (d).

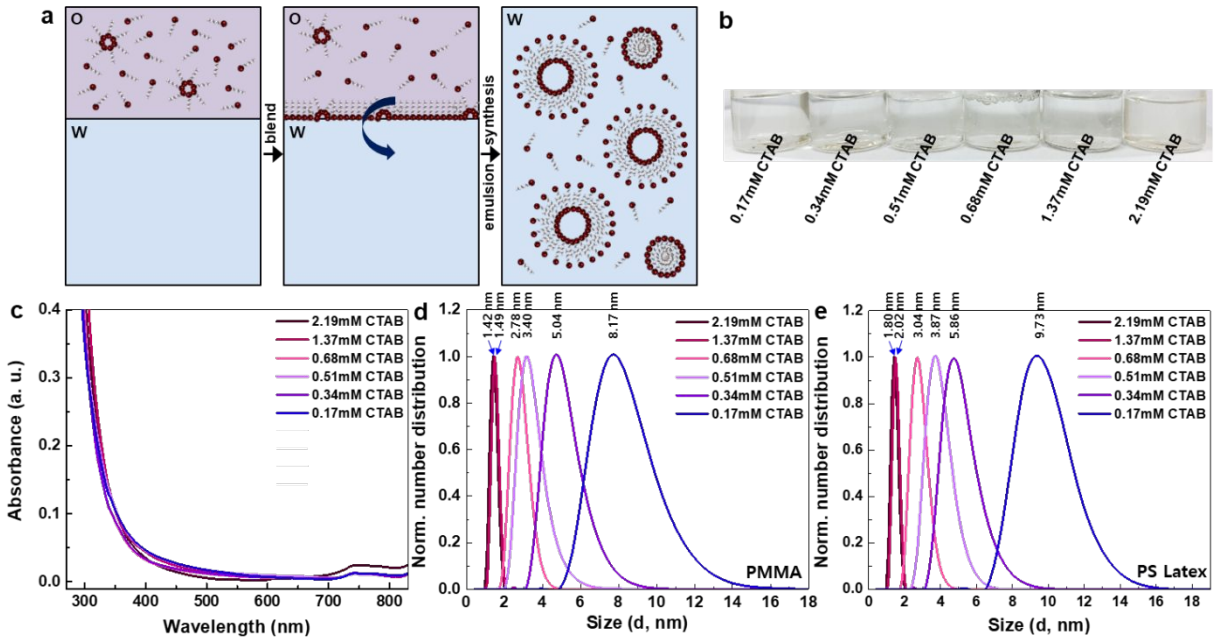

Figure S10. CTAB concentration-dependent aqueous CTAB dispersions processed with emulsion/solvent evaporation method: (a) schematic illustration of the synthesis, (b) visualization of synthesized solutions, (c) UV-vis absorption spectra, (d and e) size distributions measured by DLSs with two different structure models, PMMA (d) and PS latex (e).

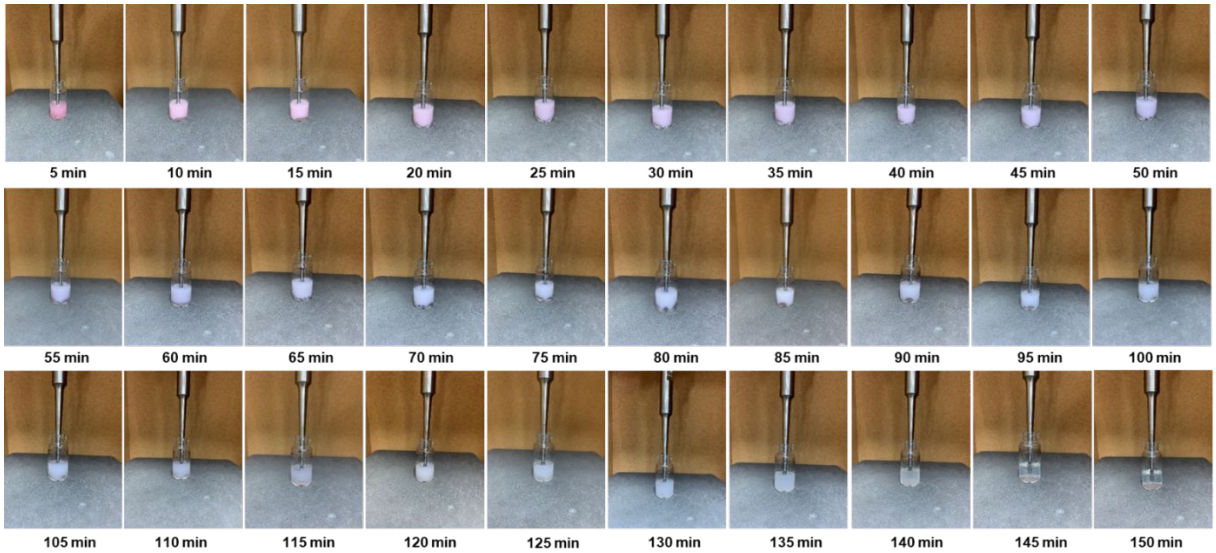

Figure S11. Snap-shots of solution color transition at each synthesis state with a time interval of 5 min in the emulsion synthesis with aqueous AuNPs and chloroform.

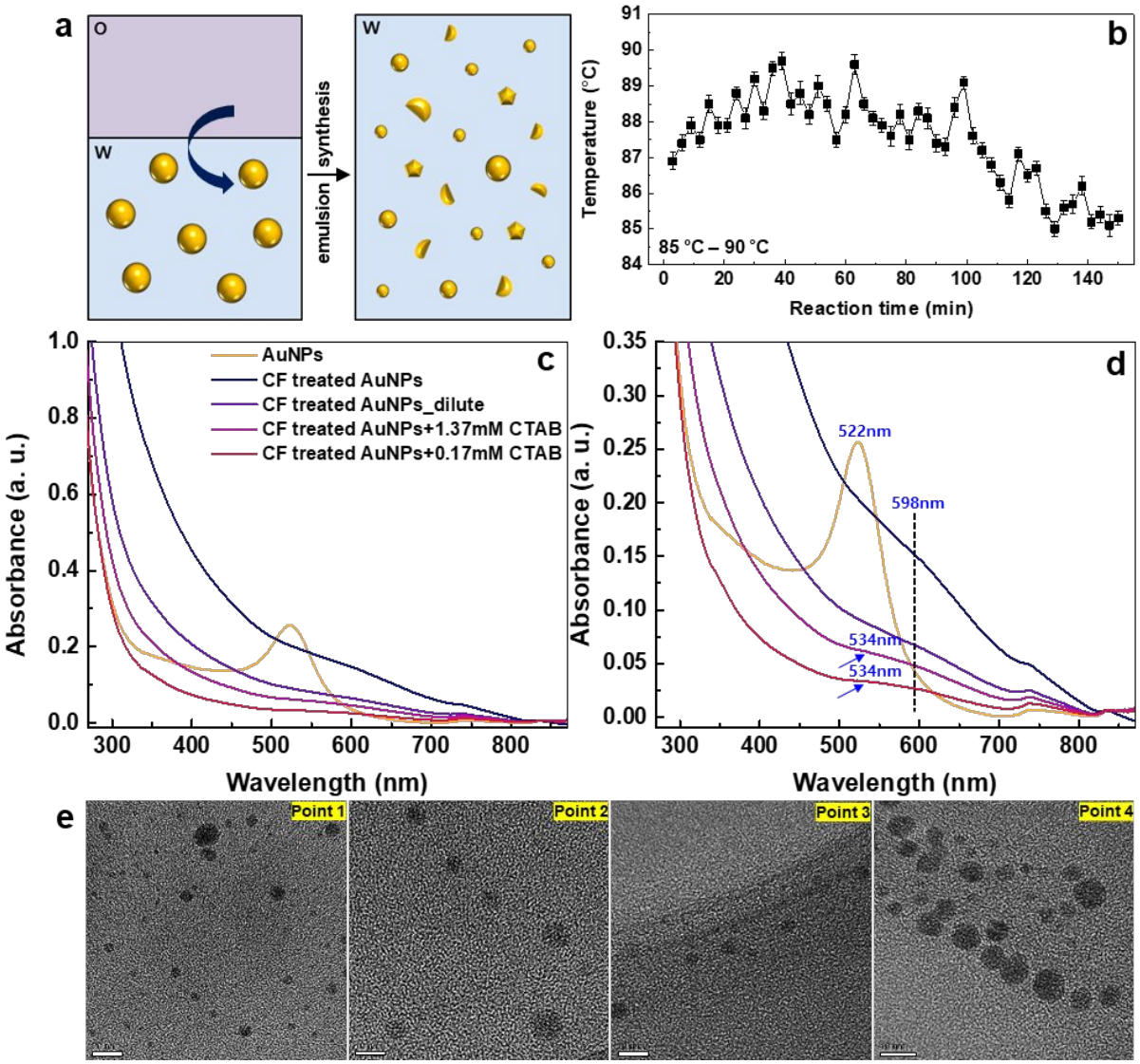

Figure S12. Aqueous AuNP dispersion treated with chloroform (CF) via the emulsion/solvent evaporation process: (a) illustrated simple synthesis process, (b) temperature scan in the synthesis, (c-d) UV-vis absorption spectra including CF treated AuNP solutions added CTAB molecules of 1.37 mM or 0.17 mM (solution: 1.27×10^{-3} M concentration and dilute solution: 1.31×10^{-6} M concentration), and (e) TEM images for cracked AuNPs under 8 nm in size at four different points (scale bars indicate 20 nm for point 1 and 10 nm for other three points).

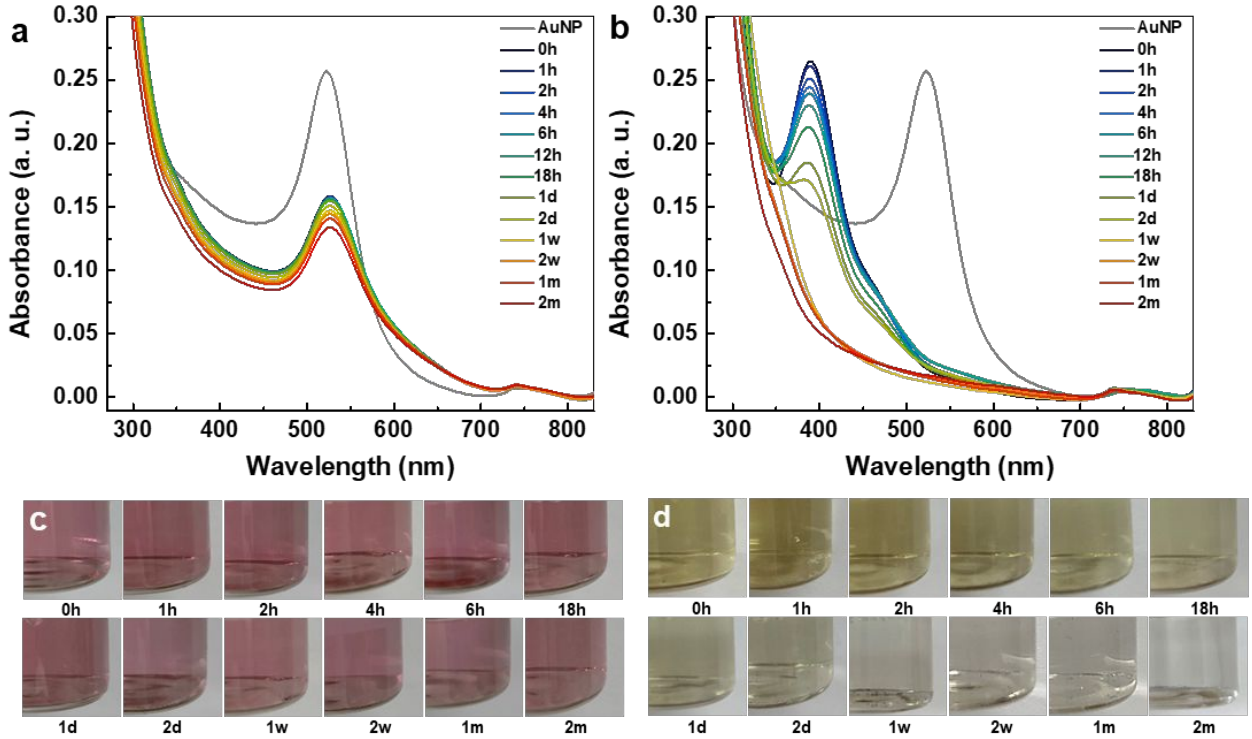

Figure S13. CTAB-loaded AuNP solutions with a 0.51 mM (a and c) or 0.17 mM (b and d) of CTAB concentration: (a and b) time-dependent Uv-vis absorption spectra and (c and d) time-dependent photo-shot images of final solutions.

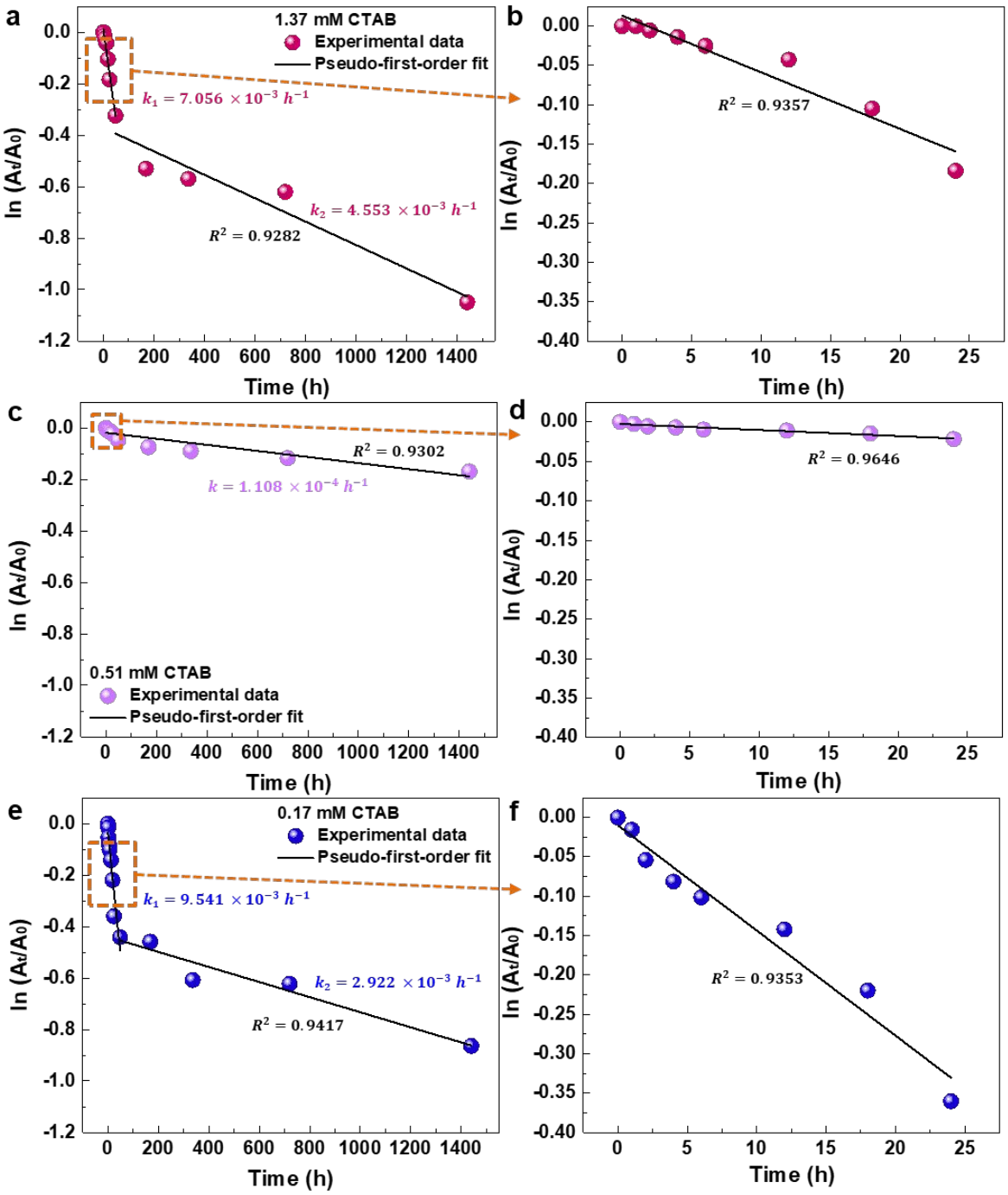

Figure S14. Detailed fitting experimental data of absorption kinetics with pseudo-first-order model for CTAB-loaded AuNPs having CTAB amount of 1.37 mM (a-b), 0.51 mM (c-d), and 0.17 mM (e-f). (b, d, and f) Magnified results from a, c, and e with a time range of 0 – 25 h.

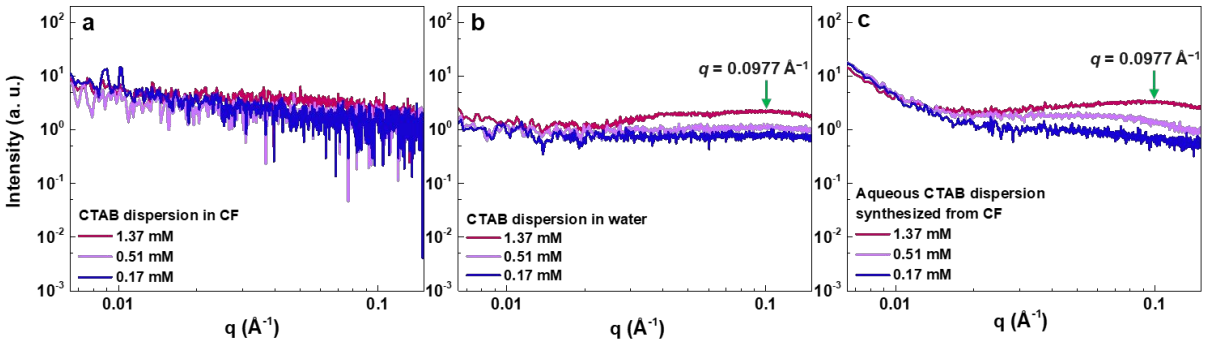

Figure S15. Transmission SAXS patterns for determining CTAB structures as a function of concentration: (a) dispersion in CF, (b) dispersion in water, and (c) dispersion synthesized using emulsion/solvent evaporation method (aqueous phase: none and oil phase: CTAB).

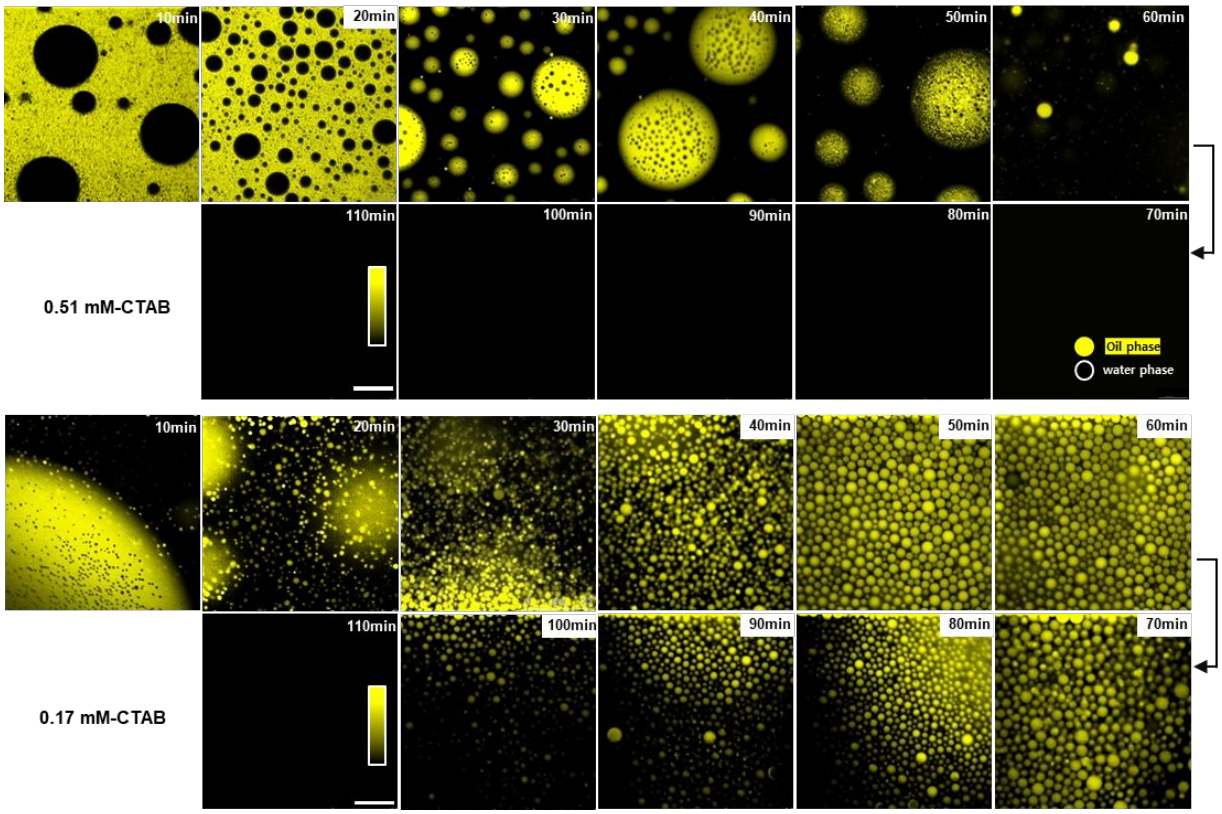

Figure S16. Time-dependent confocal microscope images of emulsions in the CTAB-loaded AuNP solutions, which measured in a time interval of 10 min: two lines in the 1st section – 0.51 mM of CTAB condition, and two lines in the 2nd section – 0.17 mM of CTAB condition. The oil phase (yellow part) was stained with a fluorescence dye, Nile red of 0.1 mg mL^{-1} (black part is an aqueous phase). The scale bar was depicted to 10 μm.

In the 0.51 mM of CTAB concentration, W/O emulsion droplets were generated at the early stage (10 min), and a phase inversion to the W/O/W emulsion state occurred at 30 min in the CTAB-covered AuNPs sample. The assembled structure of water droplets in the W/O/W emulsion state was not observed. The changed states were kept until the final form at 70 min. We find that, in this medium CTAB concentration, chemical interactions of oil and water phases before 70 min allow the CTAB-covered particle structure instead of the decomposition of aqueous material. In the 0.17 mM of CTAB condition, an emulsion droplet has a W/O/W emulsion state at the initial synthesis time (10 min) (a large oil droplet (radius = ca. 30 μm)

containing spherical small water phases). The W/O/W emulsion droplet is in the same state as the 1.37 mM of CTAB condition. The longer reaction time allowed to split the droplet into smaller-sized structures, the spherical oil phases were gradually assembled. A closely packed structure with 2 μm-sized circular droplets was finally generated at 50 min. After that time, the droplets gradually disappeared along with the evaporation of the oil phase (70 – 110 min).

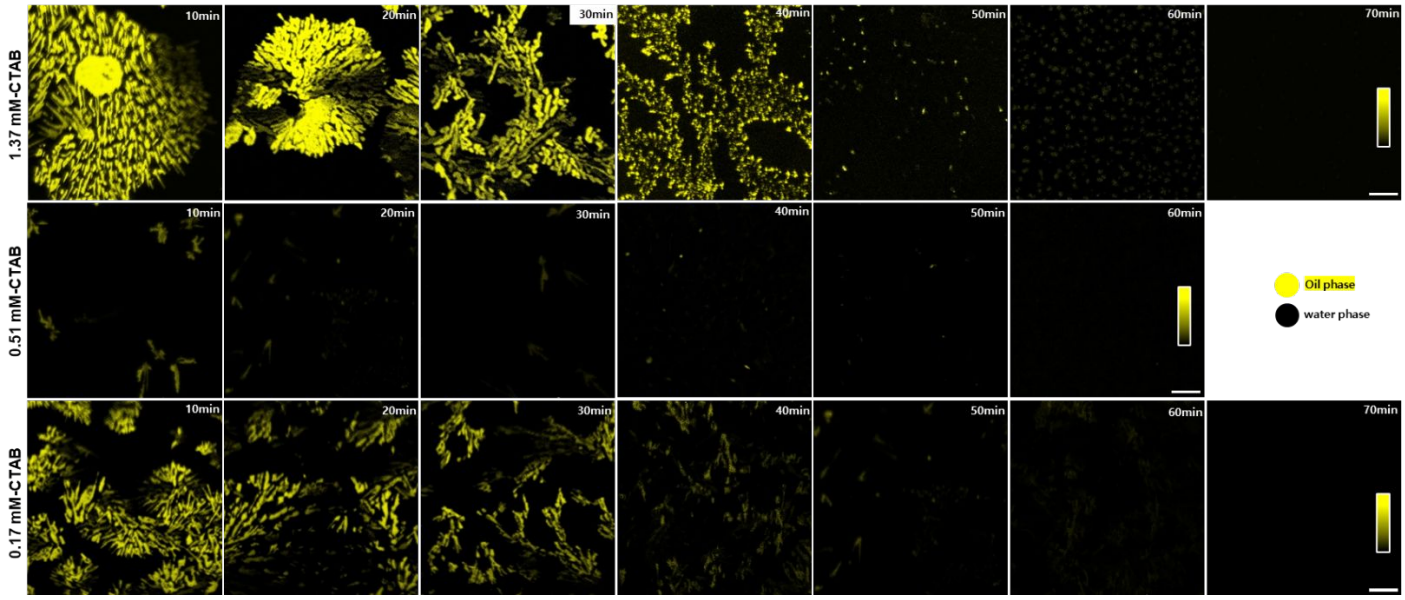

Figure S17. Time-dependent fluorescence confocal microscopy images of CTAB-loaded AuNP films in the intermediate states of emulsion/solvent evaporation synthesis: 1.37 mM of CTAB concentration (first row), 0.51 mM of CTAB concentration (second row), and 0.17 mM of CTAB concentration (third row). The oil phase was stained with a fluorescence dye, Nile red of 0.1 mg mL^{-1}. Scale bar shows 10 μm.

In the film results (Figure S17), the surfactant conditions cause chemical interactions of the oil phase with larger micro-sized domains are 1.37 mM and 0.17 mM of CTAB concentration. In the 0.51 mM of CTAB condition, however, the micron-sized network of the oil phase was not observed, demonstrating that mostly nano-sized oil phases have chemical communications with the water phase in the emulsion. The data thereby suggest that the oil phase that causes the decomposition of AuNPs has over tens of micrometer in size.

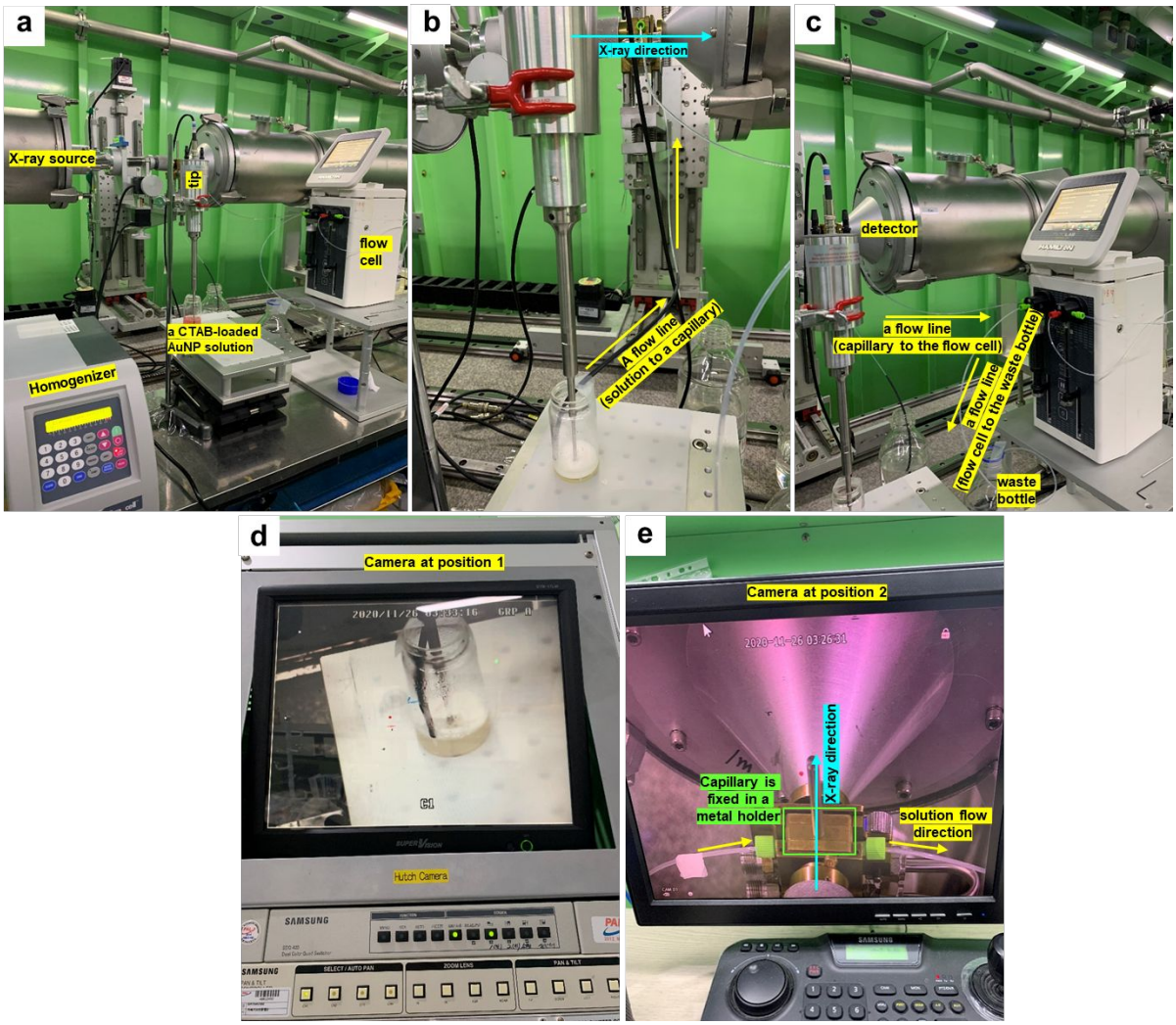

Figure S18. Experimental setup for in-situ small-angle X-ray scattering[S6-S7] to investigate the structural variation of CTAB (1.37 mM)-loaded AuNPs in the synthesis process using the emulsion/solvent evaporation method: (a) a full shot connected with synthesis equipment (homogenizer) and a flow cell, (b-c) focused shots for a detailed description for all solution flow lines and the X-ray position, and (d-e) two camera shots to confirm the solution status (d) and the solution flow (e) during the X-ray measurement.

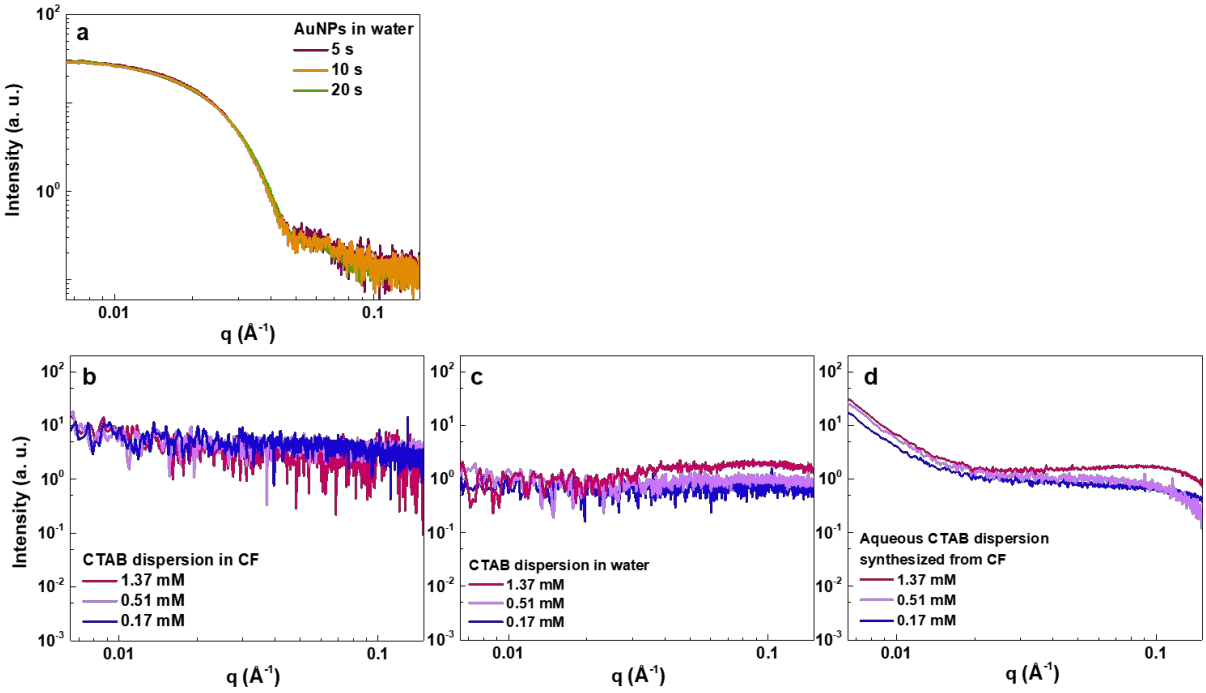

Figure S19. SAXS profiles with a static measurement: (a) AuNPs dispersed in water with an X-ray exposure time of 5 s, 10 s, and 20 s. (b) CTAB dispersion in CF, (c) CTAB dispersion in water, and (d) aqueous CTAB dispersion synthesized from CF, the same system shown in Figure S15 (a), (b) and (c), respectively, but with 20 s X-ray exposure time.

Before conducting in situ X-ray measurements, the X-ray beam damage effect for the samples was investigated with static measurements. As shown in Figure S19a, the 20 nm-sized AuNPs dispersed in water provide the same scattering results in all exposure times of 5 s, 10 s, and 20 s. Figure S19b-d show the same systems in Figure S15 with 20 s exposure; (b) CTAB solution dispersed in the CF, (c) CTAB solution dispersed in the water, and (d) dispersion synthesized using emulsion/solvent evaporation method (aqueous phase: none and oil phase: CTAB). Three different solutions have various CTAB concentrations. The patterns showed almost the same results as in Figure S15. There is no X-ray beam damage for both AuNPs and CTAB molecules up to 20 s exposure time from all data. We thereby used the 5 s X-ray exposure in the in situ measurement to get a good enough signal to noise without damage.

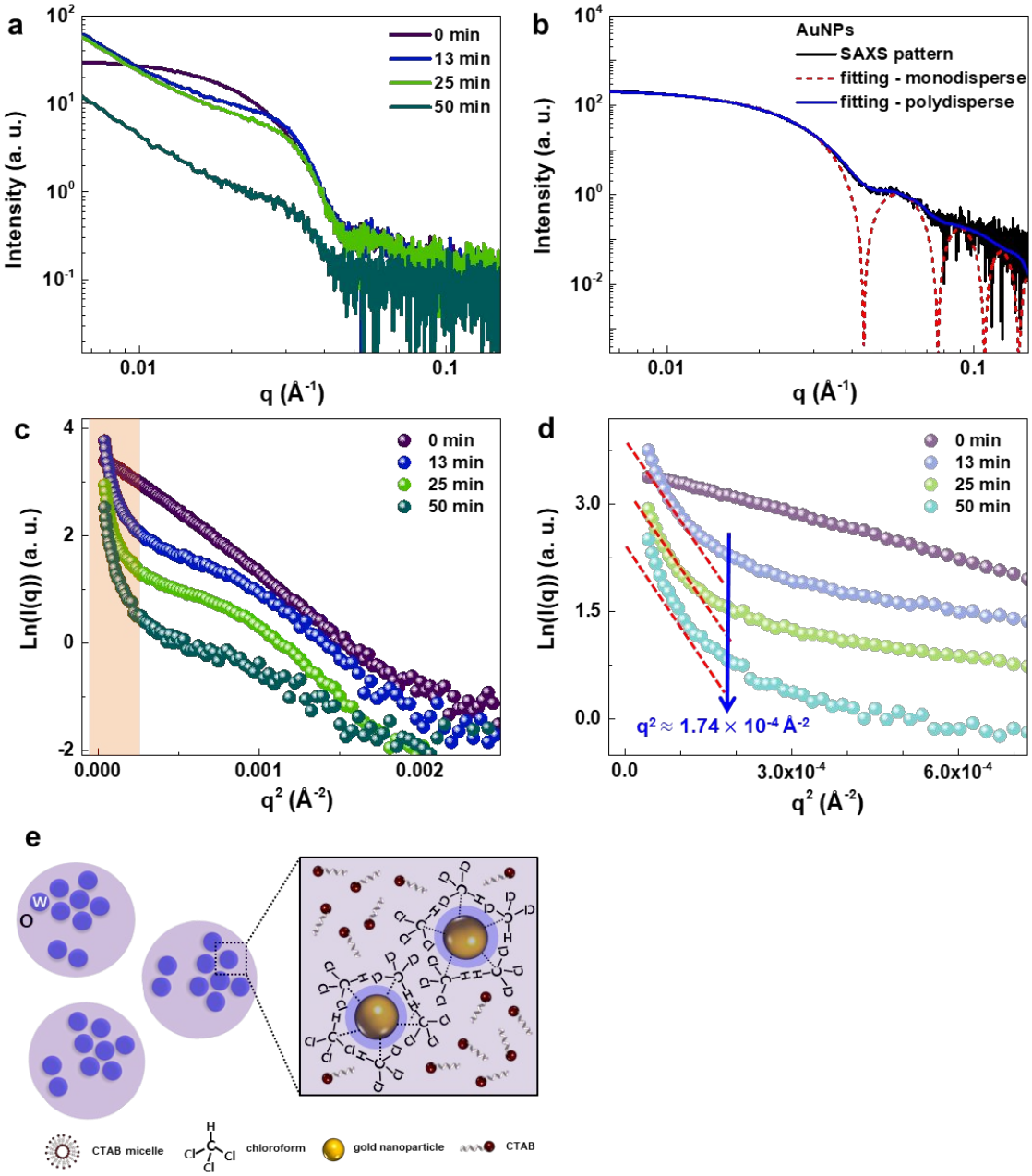

Figure S20. (a) SAXS patterns for the selective time (0, 13, 25, and 50 min), (b) SAXS fittings with two models for AuNPs, (c) Guinier plots with an area (orange box) show the strong upturn scattering in the very low *q* region arising from the large droplets. (d) The scattering profiles can be classified to two *q* regions, i.e., 3.83×10^{-5} Å^{-2} < $q^2 \leq 1.74 \times 10^{-4}$ Å^{-2} and $q^2 > 1.74 \times 10^{-4}$ Å^{-2}. Red dashed lines are the guidelines with a slope of large emulsion droplets. (e) A model for the large droplets – O/W emulsion droplets with hundred nanometers to micron-size. Aqueous AuNPs are surrounded by CF molecules and a large CF droplet has aggregated

AuNPs.

We plotted the SAXS patterns for the selective time (0, 13, 25, and 50 min) from Figure 4c (Figure S20a). For the data at 0 min (Figure S20b), the SAXS pattern shows a plateau curve in the low *q* region, which enables the data to estimate the size and structure of the AuNPs with a fitting. When the plot was fitted by a solid sphere model[S8-S9], a fitting with a modest polydispersity in size (20.0 ± 1.02 nm) with Gaussian distribution (solid blue line) was obtained. It can be compared with the monodisperse spheres with 10 nm radius (*r*) (red dash line).

However, the SAXS profiles from 13, 25, and 50 min with emulsion droplets have a gradual upturn scattering feature in the low *q* region (Figure S20c) (emulsion droplets are the large CF particle with hundred nanometers to micron-size including the aqueous AuNPs inside). To determine the large particle scattering in the pattern, the Guinier plots obtained from Figure 4d are shown (Figure S20c-d). We found a quite strong upturn scattering intensity in the very low *q* region (orange box in Figure S20c) and classified two scattering sections based on the q^2 value of 1.74×10^{-4} Å^{-2}, i.e., 3.83×10^{-5} Å$^{-2} < q^2 \leq 1.74 \times 10^{-4}$ Å^{-2} (red dash-line region) and $q^2 > 1.74 \times 10^{-4}$ Å^{-2} (Figure S20d). We guess that the large particle to an emulsion droplet is responsible for the increase in the intensity at low *q*. A CF droplet with hundred nanometers to micron-size has the aggregated aqueous AuNPs. In other words, aqueous AuNPs are surrounded by CF molecules, an oil (O)-water (W) emulsion droplet is formulated (Figure S20e).

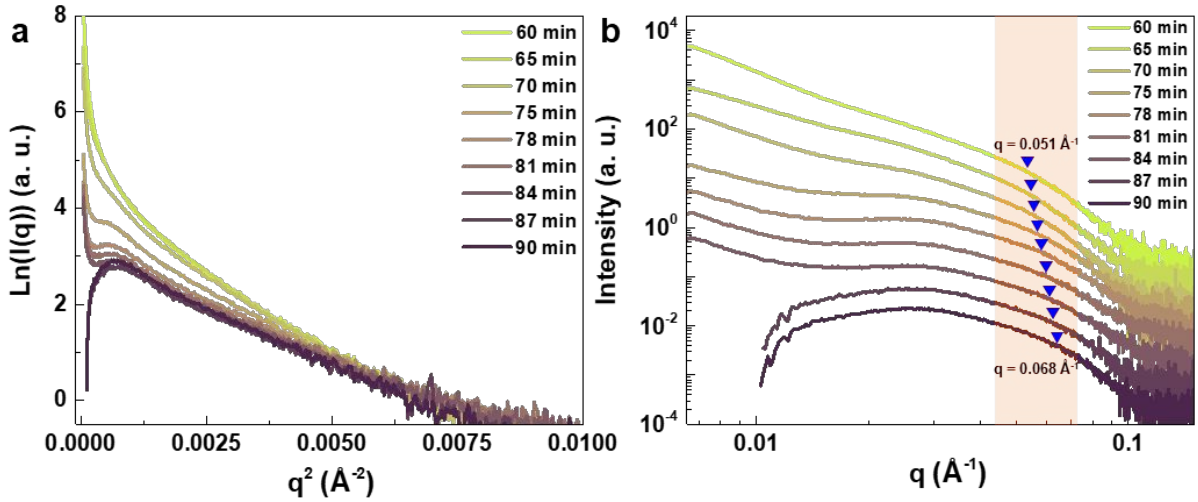

Figure S21. Extracted data from Figure 4b: (a) Guinier plots and (b) Intensity, $I(q)$ versus wavevector q curves obtained by radial integration of the 2D SAXS patterns with a time range from 60 min to 90 min. The blue triangle marks, including a square region, highlight a shift of scattering features from $q \approx 0.051$ Å^{-1} to $q \approx 0.068$ Å^{-1}.

Table S1. Detailed Soret peak positions in the UV-vis absorption spectra of Figure 2d.

Time	Wavelength (nm)	Intensity (a. u.)
0h	389.76	0.2542
1h	389.76	0.2541
2h	389.64	0.2528
4h	389.47	0.2507
6h	388.96	0.2479
12h	388.18	0.2436
18h	387.01	0.2289
1d	386.41	0.2115
2d	385.14	0.1838
1w	375.56	0.1496
2w	360.26	0.1438
1m	359.50	0.1367
2m	355.03	0.0890

Table S2. Detailed LSPR band positions in the UV-vis absorption spectra of CTAB (0.51mM)-capped AuNP solution.

Time	Wavelength (nm)	Intensity (a. u.)
0h	526.06	0.1583
1h	526.05	0.1579
2h	526.12	0.1574
4h	526.13	0.1572
6h	526.18	0.1568
12h	526.20	0.1566
18h	526.21	0.1560
1d	526.29	0.1549
2d	526.33	0.1508
1w	526.42	0.1469
2w	526.54	0.1446
1m	526.62	0.1408
2m	526.66	0.1336

Table S3. Detailed variation for Soret band positions in the UV-vis absorption spectra of $AuBr_4$-CTA complex solution with a 0.17 mM of CTAB.

Time	Wavelength (nm)	Intensity (a. u.)
0h	389.75	0.2650
1h	389.56	0.2609
2h	389.37	0.2511
4h	389.18	0.2443
6h	388.83	0.2394
12h	388.46	0.2299
18h	388.27	0.2127
1d	387.20	0.1848
2d	386.64	0.1704
1w	353.90	0.1675
2w	353.28	0.1443
1m	353.28	0.1422
2m	353.28	0.1117

References

(S1) Schmid, B.; Schindelin, J.; Cardona, A.; Longair, M.; Heisenberg, M. A High-level 3D Visualization API for Java and ImageJ. *BMC Bioinformatics* **2010**, *11*, 274. DOI: 10.1186/1471-2105-11-274

(S2) Li, R.; Wang, Z.; Gu, X.; Chen, G.; Zhang, Y.; Hu, D. Study on the Assembly Structure Variation of Cetyltrimethylammonium Bromide on the Surface of Gold Nanoparticles. *ACS Omega*, **2020**, *5*, 4943-4952. DOI: 10.1021/acsomega.9b03823

(S3) Lim, J.; Lee, N. – E.; Lee, E.; Yoon, S. Surface Modification of Citrate-Capped Gold Nanoparticles Using CTAB Micelles. Bull. Korean Chem. Soc. 2014, 35, 2567-2569. DOI:10.5012/bkes.2014.35.8.2567

(S4) Jiang, Z.; He, J.; Deshmukh, S. A.; Kanjanaboos, P.; Kamath, G.; Wang, Y.; Sankaranarayanan, K. R. S. S.; Wang, J.; Jaeger, H. M.; Lin, X. -M. Subnanometer Ligand-Shell Asymmetry leads to Janus-like Nanoparticle Membranes. *Nat. Mater*., **2015**, *14*, 912-917, DOI:10.1038/nmat4321

(S5) Fong, K. E.; Yung, L. -Y. L. Localized Surface Plasmon Resonance: A Unique Property of Plasmonic Nanoparticles for Nucleic Acid Detection. *Nanoscale* **2013**, *5*, 12043-12071. DOI: 10.1039/C3NR02257A

(S6) Kwon, S. G.; Krylova, G.; Phillips, P. J.; Klie, R. F.; Chattopadhyay, S.; Shibata, T.; Bunel, E. E.; Liu, Y.; Prakapenka, V. B.; Lee, B.; Shevchenko, E. V. Heterogeneous Nucleation and Shape Transformation of Multicomponent Metallic Nanostructures. *Nat. Mater.*, **2015**, *14*, 215-223, DOI: 10.1038/nmat4115

(S7) Brotherton, E. E.; Hatton, F. L.; Cockram, A. A.; Derry, M. J.; Czajka, A.; Cornel, E. J.; Topham, P. D.; Mykhaylyk, O. O.; Armes, S. P. In situ Small-Angle X-ray Scattering Studies During Reversible Addition-Fragmentation Chain Transfer Aqueous Emulsion Polymerization.

J. Am. Chem. Soc. **2019**, 141, 13664–13675. DOI: 10.1021/jacs.9b06788

(S8) Ingham, B.; Li, H.; Allen, E. L.; Toney, M. F. SAXSFit: A Program for Fitting Small-Angle X-ray and Neutron Scattering Data. arXiv:0901.4782.

(S9) Wang, W.; Zhang, H.; Kuzmenko, I.; Mallapragada, S.; Vaknin, D. Assembling Bare Au Nanoparticles at Positively Charged Templates. *Sci. Rep.*, **2016**, *6*, 26462. DOI: 10.1038/srep26462.

Full references in the main text

(14) Kim, K. H.; Kim. S.; Ryu, J.; Jeon, J.; Jang, S. G.; Kim, H.; Gweon, D. -G.; Im, W. B.; Han, Y.; Kim, H.; Choi, S. Q. Processable High Internal Phase Pickering Emulsions using Depletion Attraction. *Nat. Commun*. **2017**, *8*, 14305. DOI:10.1038/ncomms14305